Dissolution of Spinel Oxides and Capacity Losses in 4 V $Li/Li_xMn_2O_4$ Cells

Dong H. Jang, Young J. Shin, and Seung M. Oh*

Department of Chemical Technology, College of Engineering, Seoul National University, Seoul 151-742, Korea

ABSTRACT

Dissolution of spinel manganese oxides and the concomitant cathodic capacity losses were examined in 4 V Li/PC + DME + $LiClO_4/Li_xMn_2O_4$ cells where PC is propylene carbonate and DME is dimethoxyethane. Dissolved Mn^{2+} contents in the electrolytes were analyzed as a function of cathode potential and carbon contents in the composite cathodes. Characteristically, manganese dissolution was notably high at the charged state (at >4.1 V *vs.* Li/Li^+), in which potential range an electrochemical oxidation of the solvent molecules was also prominent. From this and another observation whereby the Mn dissolution increased with increasing carbon content in the composite cathodes, it was proposed that, at the charged state of the cathode the solvent molecules are electrochemically oxidized on carbon surfaces and an as-generated species promotes the manganese dissolution. Results of an ac impedance study revealed that Mn dissolution brings about an increase in contact resistances at the Mn-depleted spinel/carbon interface, and also in the electrode reaction resistances for Li^+ intercalation/deintercalation. Thus, the Mn dissolution causes capacity losses in two different pathways; material loss of the loaded spinel and polarization loss due to a cell resistance increment. The former prevailed when cathodes contained excess amounts of carbon, while the latter became more of a problem as the carbon contents decreased.

Introduction

The spinel $Li_xMn_2O_4$ has been widely studied for rechargeable Li batteries.[1-13] When Li^+ ions are intercalated/deintercalated in the range of $x = 0$ to 1.0, the output potential of the $Li/Li_xMn_2O_4$ cell is about 4 V (*vs.* Li/Li^+), whereas when $1 < x < 2$, the cell discharges at about 3 V. The cyclability in these cells is closely related with structural variations evolved during the charge/discharge cycling. When the cells discharge within the 4 V range, the cubic symmetry of the spinel oxides is retained, therefore the lattice expansion and contraction proceeds isotropically to give minimal stress on the crystal lattices.[4-6] On the contrary, when the spinel electrodes are deeply discharged in the range of $x = 1.0$ to 2.0, the average oxidation state of manganese ions is lowered to less than 3.5, and the crystal symmetry changes from cubic to tetragonal phase accompanied by an increment in the c/*a* ratio of the unit cell (Jahn-Teller distortion).[7-9] This structural distortion is too large for the spinel framework to maintain its structural integrity, leading to a capacity loss with repeated cycling. Consequently, the 4 V cells show better cyclability than the 3 V cells.

The spinel manganese oxides have been tested as 4 V cathode materials, and some attractive properties have been reported.[11,12] Nevertheless, a slow capacity fade upon repeated charge/discharge cycling has been observed even in many 4 V cells.[13] The origin of this capacity loss has not been clarified, but some suspected candidates have been proposed[13]: (*i*) an electrochemical reaction of electrolytes on the electrode at the charged state, (*ii*) a slow dissolution of spinels according to the disproportionation reaction: $2\ Mn^{3+} \rightarrow Mn^{4+} + Mn^{2+}$, and (*iii*) a structural transition due to Jahn-Teller distortion at the discharged state.

The prime concern in this study was the identification of the origin of cathodic capacity losses encountered in 4 V $Li/Li_xMn_2O_4$ cells. First of all, in order to accomplish this goal, spinel oxides with different surface areas were prepared, and their cyclabilities were compared with each other. As a result of this study, manganese dissolution was shown to be the primary reason for the capacity loss. Also, results indicated that manganese dissolution varies with the cathode potential and carbon contents in the composite cathodes, and it is also closely related with the electrochemical oxidation of solvent molecules on carbon additives. An ac impedance study was carried out to analyze the effects that manganese dissolution has on the electrochemical properties of the composite cathodes and their cyclabilities.

* Electrochemical Society Active Member.

Experimental

Materials.—Powders of lithium manganese oxides were prepared by the citrate gel method.[14,15] To this end, a mixture of $LiNO_3$ (Aldrich, 99.99%, 20 mmol), $Mn(NO_3)_2\ 6H_2O$ (Aldrich, 98%, 40 mmol), and citric acid (Aldrich, >99.5%, 60 mmol) was dissolved in water. The resulting aqueous solutions were then concentrated to give sols and further dried in vacuum to yield amorphous gels. The gels were then crushed and calcined at 600 to 800°C for 4 h. The heating and cooling rates were fixed at 1 and 0.5°C min^{-1}, respectively. The surface area of the powder materials was measured by Brunauer, Emmett, and Teller (BET) techniques. The total Mn content and average Mn valence of the oxides were determined by potentiometric titration methods as reported in the literature.[16,17] The electrolyte used was a 1:1 mixture of propylene carbonate (PC) and dimethoxyethane (DME) containing 1 *M* $LiClO_4$ (Mitsubishi Co.).

To prepare the composite cathodes, spinel powders were mixed with acetylene black (Vulcan XC-72) and Teflon binder with different weight ratios, depending on the objective of the experiments. The mixtures were then dispersed in isopropyl alcohol and spread on Exmet (1 cm^2), followed by pressing and drying at 120°C for 3 h.

Battery performance was tested in a beaker-type three-electrode cell, where Li foil (Cyprus Co.) was used as the anode and reference electrode. Normally, 15 mg cm^{-2} of spinel powder (8.3×10^{-5} equiv.) was loaded in the cathodes and 100 mg of Li foil (1.4×10^{-2} eq) was used as the anode. Hence, the $Li/Li_xMn_2O_4$ cells tested in this study were cathode-limited such that the observed capacity values represented those of the spinel oxides. In addition, since dissolved Mn ions were deposited on the Li anode and reference electrodes,[18,19] the reference electrode was isolated from the cathode by a Vycor tip and the anode by a fritted glass. With this cell configuration, a darkening of the Li electrodes (deposition of Mn on Li electrode surface) can be eliminated, enabling us to estimate the extent of Mn dissolution by an analysis of the electrolyte alone.

Instrumentations.—The charge-discharge profiles were recorded in the beaker-type cell with a home-made instrument. The cutoff potentials for the charge and discharge limit were fixed at 4.3 and 3.6 V (*vs.* Li/Li^+), respectively. The charge/discharge cycling was performed galvanostatically with a current density of 1 mA cm^{-2}. Dissolved Mn^{2+} ions in the electrolytes were analyzed with differential pulse polarography.[20,21] For this, EG&G Princeton Applied Research Model 174A polarographic analyzer and Model 303 SMDE were utilized. A tartaric acid/ammonium hydroxide buffer (pH 9.0) was employed as the electrolyte.

AC impedance measurements were made over the frequency range of 0.005 Hz to 100 kHz using EG&G M173 potentiostat, M276 interface, and 5208 lock-in analyzer. Spectra were obtained at the open-circuit condition after discharge down to 3.6 V. Deconvolution of the complex impedance spectra was performed with commercially available software.[22] For the electrochemical potential spectroscopy[23,24] measurement, EG&G M362 potentiostat and programmable potential source were combined to control the applied potential step, and the current was continuously monitored until it decayed to a preset threshold value ($I_{threshold}$ = 0.0013 mA). The cell potential was increased stepwise by dV (=0.01 V). All the experiments were carried out at ambient temperature in a dry box filled with argon.

Results and Discussion

Characterization of spinel materials.—Table I lists the powder properties of as-obtained spinels such as surface area, total Mn content, and average Mn valence. Also the cathodic properties such as initial open-circuit potential and initial charge capacity were included. The 800°C fired spinel showed an average Mn valence of 3.53 (the lowest value among the samples) and therefore the lowest initial open-circuit potential (3.3 V *vs.* Li/Li^+). As expected, this spinel exhibited the highest initial charging capacity (up to 4.3 V). The reverse trends can be seen in the lower temperature fired samples.

X-ray powder diffraction analyses of the prepared powders indicated a spinel structure with no discernable impurities. However, the diffraction peaks were broader in the lower temperature calcined spinels. Many oxygen-rich defect spinels are known in Li-Mn-O system.[13] The spectrum of oxygen richness ranges from the regular stoichiometric spinel ($LiMn_2O_4$) to $Li_2Mn_4O_9$ and further to $Li_4Mn_5O_{12}$. The lattice parameters of the regular spinel and some of the oxygen-rich defect spinels are listed in Table II. As can be seen in the table, the lattice parameter decreases with increasing oxygen content. The listed numbers (lattice parameter, oxygen nonstoichiometry, and Mn valence) for the 800°C calcined spinels are very close to those of the regular stoichiometric spinel. But with decreasing calcination temperature, the oxygen content steadily increased to reach δ = 0.11 for the 600°C powders. Clearly, this observation supports the earlier finding[13] that oxygen-rich spinels are formed at lower temperatures. It is thus likely that the higher Mn valence and the broader diffraction peaks of the spinels prepared at lower temperatures are due to an incomplete conversion to the stoichiometric spinel phase. However, even in the 600°C calcined spinel, a possible contamination by the highly oxygen-rich defect spinels ($Li_2Mn_4O_9$ or $Li_4Mn_5O_{12}$), which are known to have little or no capacity above 3 V (*vs.* Li/Li^+),[13] seems to be negligible as its lattice parameter and Mn valence deviate far from those of the inactive spinels. Meanwhile, spinel powders with δ = 0.1 which have the similar composition to the 600°C powders are known to be active in 4 V range.[13]

Dissolution of manganese oxides.—Figure 1 shows the discharge capacity profiles of the $Li/Li_xMn_2O_4$ cells according to cycle number, where the spinels calcined at three different temperatures were loaded in each cathode.

Table I. Powder and cathode properties observed with spinel manganese oxides calcined at different temperatures.

Calcination temperature (°C)	Surface area[a] (m^2g^{-1})	Total Mn content[b] (%)	Average oxidation state of Mn	Initial open circuit potential (V)	Initial charge capacity (mAh g^{-1})
600	21.20	58.24	3.61	3.45	124
700	11.89	59.68	3.55	3.36	131
800	3.64	59.91	3.53	3.30	134

[a] Measured by BET method (N_2 adsorption).
[b] Calculated by potentiometric titration.

Table II. The lattice parameter and average Mn valence of various spinel manganese oxides.

Composition of spinel phase	δ	Lattice parameter a (Å)	Average Mn valence	Ref.
$LiMn_2O_4$		8.245	3.50	7
		8.232	3.50	13
$LiMn_2O_{4+\delta}$				
800°C fired	0.03	8.244	3.53	This work
700°C fired	0.05	8.240	3.55	This work
600°C fired	0.11	8.233	3.61	This work
$LiMn_2O_{4+\delta}$	0.10	8.218	3.60	13
$Li_2Mn_4O_9$		8.162	4.00	7, 13
$Li_4Mn_5O_{12}$		8.137	4.00	7, 13

One feature to be noted in Table I and Fig. 1 is that the spinel oxides calcined at higher temperatures have smaller surface areas but show a better capacity retention in this cycling regime (3.6 to 4.3 V). For example, the 800°C calcined spinel (surface area = 3.64 m^2/g^{-1}) shows a discharge capacity amounting to 83% of the initial value even after 60 cycles, while with the 600°C calcined oxide (surface area = 21.2 m^2/g^{-1}) the capacity is reduced to half of the initial value. The 600°C calcined spinels were collected after 60 cycles and analyzed with x-ray diffraction (XRD). There were no diffraction peaks belonging to tetragonal phases; therefore, a possible contribution from Jahn-Teller distortion has been excluded.

To test the spinel dissolution, the electrolytic solutions ($PC+DME/LiClO_4$) were sampled intermittently during the cycle test of $Li/Li_xMn_2O_4$ cells, and they were analyzed with differential pulse polarography.[20,21] Figure 2 represents typical polarograms recorded with the electrolytic solutions, which were sampled after the 20th (a) and 40th (c) cycle. The peak potential of *ca.* −1.5 V (*vs.* sat. Ag/AgCl) observed with the sampled electrolytes was identical to that recorded with a separately prepared Mn^{2+} solution (b).

The concentration of Mn^{2+} ions in the electrolyte was monitored during the charge/discharge cycle (Fig. 3a). As can be seen, the Mn^{2+} concentration steadily increases with repeated cycling in three cells. Evidently, however, the dissolution was the severest in the 600°C fired spinel, while the least in the 800°C calcined oxide. Obviously, this difference can be attributed to the spinel's surface area

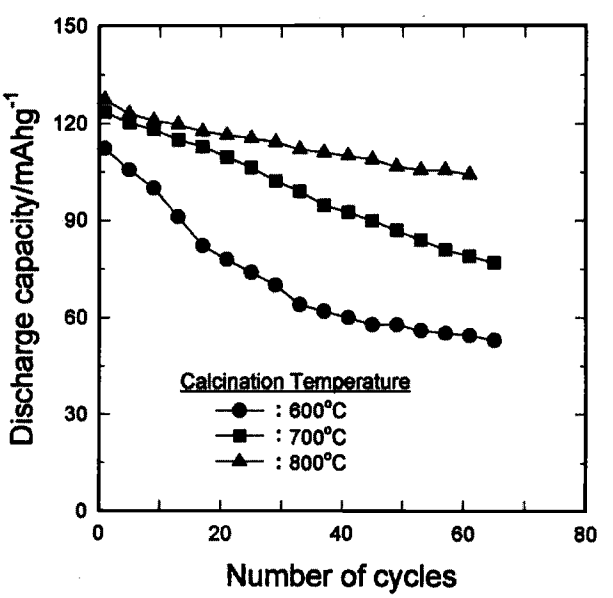

Fig. 1. Discharge capacity of $Li_2/Li_xMn_2O_4$ cells according to cycle number. Cycling was carried out galvanostatically at a current density of 1 mA cm^{-2} between 4.3 and 3.6 V. The cathodes were composed of spinel oxides, acetylene black (Vulcan XC-72), and PTFE binder (75:21:4 in weight ratio).

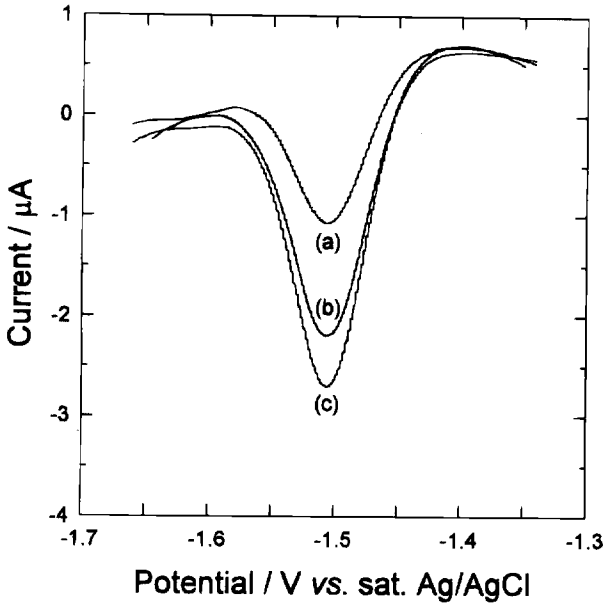

Fig. 2. Differential pulse polarograms in 0.2 *M* ammonium tartrate buffer (pH 9.0): (a) after 20th cycle of $Li/Li_xMn_2O_4$ cell, (b) recorded with 0.56 m*M* of Mn^{2+} solution, and (c) after 40th cycle. The spinel oxide was calcined at 600°C, and the cathode composition and cycling conditions were the same as those for Fig. 1.

(Table I) since Mn dissolution would take place at the spinel/electrolyte interface.

Material losses in the composite cathodes were calculated based on the Mn^{2+} concentrations in the electrolytes, and the fraction of material loss over the total was plotted in Fig. 3b. The material losses account for only 20 to 33% of the overall losses in this series of samples. This shows that the manganese dissolution has, in addition to the material loss, other unfavorable effects on the cathode properties which should account for the other portion (67 to 80%) of the capacity losses. This is discussed further in later sections.

Dissolution mechanism of $Li_xMn_2O_4$.—As stated, the spinels dissolve substantially during the charge/discharge process in the potential range of 4.3 to 3.6 V (*vs.* Li/Li^+). In order to see any potential dependence of the manganese dissolution, the composite cathodes were polarized at a fixed potential between 3.8 and 4.2 V (*vs.* Li/Li^+), and the dissolved Mn^{2+} contents were monitored as a function of time. As illustrated in Fig. 4, Mn dissolution was not appreciable when the applied potential was below *ca.* 4.0 V, but it became notably high starting from *ca.* 4.0 V. Interestingly, this potential dependence is quite similar to the current evolution of solvent oxidation on a carbon electrode as can be seen in Fig. 5, where the electrochemical potential spectroscopy differential charge is plotted as a function of electrode potential. The solvent mixture (PC + DME) was electrochemically oxidized at above 4.0 V on the carbon electrode. Since the electrochemical potential spectroscopy provides a steady-state voltammogram, the evolution of electrolyte oxidation against potential can be clearly identified without mass-transfer effects.[23,24] These two results suggest that some intermediates, generated by an electrochemical oxidation of solvent molecules on carbon surface, are deeply involved in the manganese dissolution reaction. Support for this suggestion can be found in the cyclic voltammograms recorded with the electrolyte on carbon electrode (inset of Fig. 5), where three different solvent mixtures were tested. The voltammograms tell us two features. First, the oxidation currents (forward scan in the positive direction) increase with increasing DME contents. Second, the reverse cathodic currents are appreciable and furthermore are proportional to the corresponding anodic currents. This illustrates that the oxidized species,

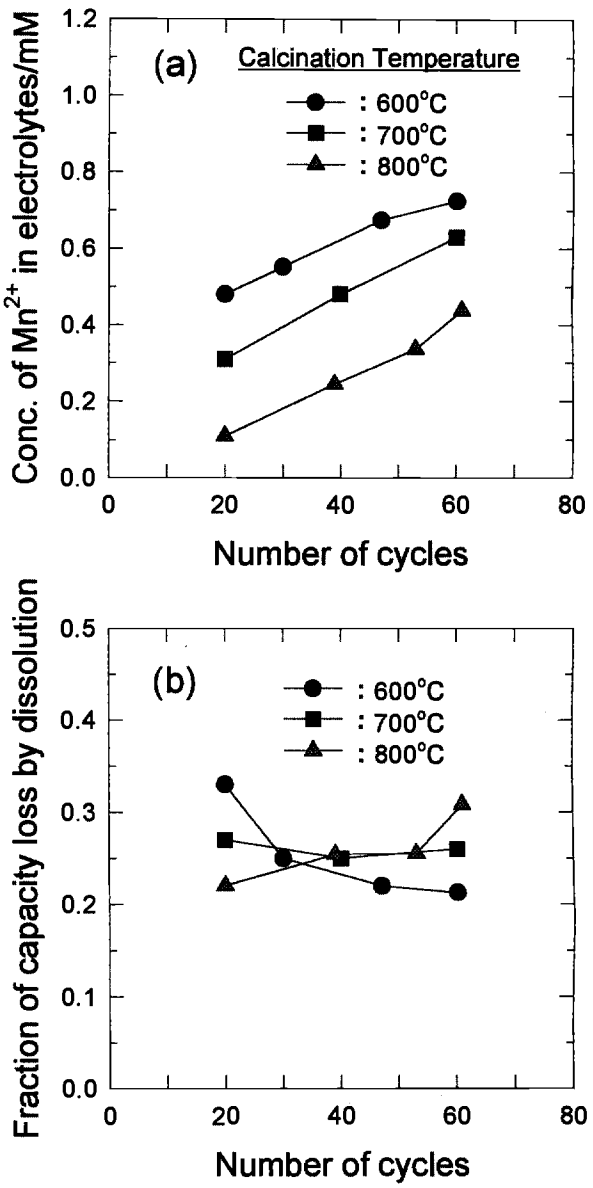

Fig. 3. (a) Concentration of Mn^{2+} ions in the electrolytes (PC/DME/1 *M* $LiClO_4$) with repeated cycling. (b) Fractional capacity losses estimated from the Mn dissolution.

derived mainly from DME, is quite stable within the experimental time scale; thus, it may participate in the dissolution reaction. Further support can be obtained from the results shown in Fig. 6. For this experiment, a carbon electrode (Vulcan XC-72:PTFE binder = 95:5 in weight ratio) and a composite electrode (spinel oxide:Vulcan XC-72:PTFE binder = 75:21:4 in weight ratio) were closely placed in the electrolyte solution. When both electrodes were left under open-circuit condition, manganese dissolution was minimal. However, when the carbon electrode was polarized at 4.2 V while the spinel-containing composite electrode under open-circuit condition, significant amounts of Mn^{2+} ions were detected in the electrolyte. This observation evidently illustrates that the solvent molecules (dominantly DME) are oxidized on the carbon electrode at >4.0 V and an as-generated species moves to the composite electrode to participate in the dissolution reaction. Until now, however, chemical actions of the solvents or their oxidation products on spinel dissolution have not been fully understood. A preliminary result indicates that the combined phenomena of solvent oxidation and spinel dissolution are quite common in most organic solvents even though the degree of spinel dissolution depends on the sol-

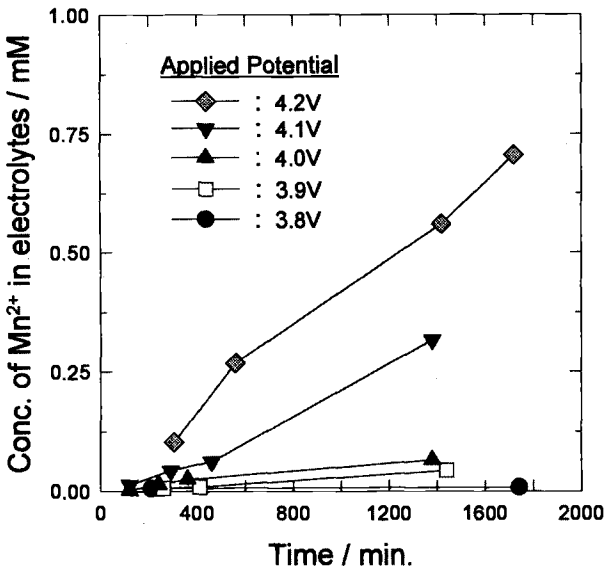

Fig. 4. Concentration of Mn^{2+} ions in the electrolytes as a function of time and cathode potentials. The composite cathode, loaded with 600°C calcined spinel, was polarized at a fixed potential, and the Mn^{2+} concentration was monitored with time.

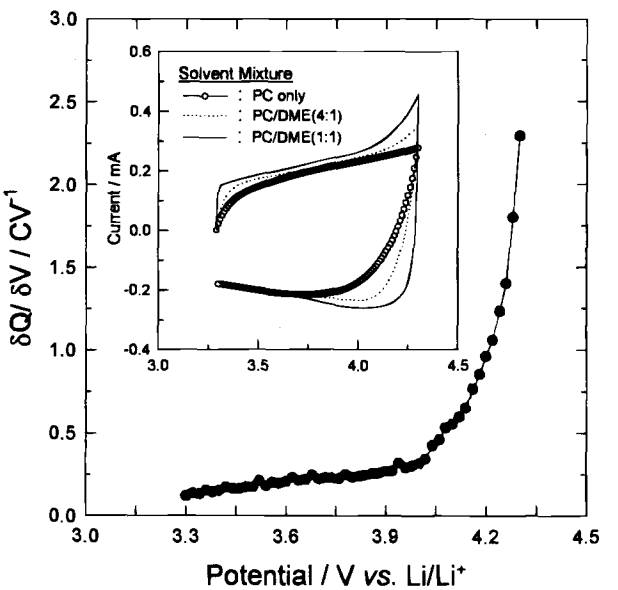

Fig. 5. Electrochemical potential spectroscopy differential charge plot recorded with carbon electrode (Vulcan XC-72: Teflon binder = 95:5 in weight ratio) in PC/DME (1:1) + 1 *M* $LiClO_4$ electrolyte. The corresponding cyclic voltammograms recorded with different solvent compositions (with 1 *M* $LiClO_4$) were presented in the inset. Scan rate = 1 mV s^{-1}.

vent. A suggestion for this may be given that the process involves organic radical species and/or acids which are

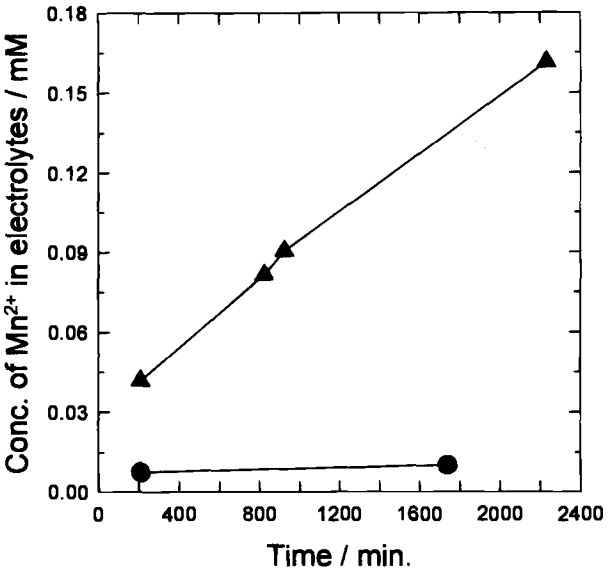

Fig. 6. Concentration of Mn^{2+} ions in the electrolyte (PC/DME/1 *M* $LiClO_4$) against the elapsed time: (●) both carbon electrode (Vulcan XC-72: Teflon binder = 95:5 in weight ratio) and composite electrode (spinel oxide: Vulcan XC-72:Teflon binder = 75:21:4 in weight ratio) were left under open-circuit conditions, and (▲) the carbon electrode was held at 4.2 V, while the composite electrode was under open-circuit condition. The two electrodes were placed as close as possible.

produced as a result of electrochemical reactions of organic solvents and/or impurities such as water. A detailed study is in process.

Meanwhile, Mn dissolution has been proposed in the literature[9,13] to proceed through a disproportionation reaction: $2\ Mn^{3+} \rightarrow Mn^{4+} + Mn^{2+}$. However, the present results indicate that this mechanism seems to be unlikely since the dissolution takes place dominantly at the end of a charging process, in which potential range the Mn^{3+} content in spinel oxides is minimal. In addition, spinel oxides may be dissolved in two different ways; dissolution of the spinel framework (both Mn and oxide ions) or Mn only with a retention of the oxide lattice. No clear evidence has been presented to differentiate this in the literature.[18,19] However, the latter may be far more likely judging from the fact that Mn-depleted (oxygen-excess) spinels are quite popular and commonly found in syntheses as described in the previous section.

Origin of capacity loss in spinel manganese oxides.— Table III summarizes the cell properties such as discharge capacity, Mn^{2+} concentration in the electrolyte, and the fractional losses contributed by the manganese dissolution. The carbon contents and calcination temperature for spinel preparation were varied. A brief look at the table indicates that the 800°C fired spinels exhibit a better capacity retention with a minimal manganese dissolution, as compared to the 600°C fired oxides. This feature has

Table III. Cell properties of the composite cathodes as functions of cycle number. Two spinel oxides (calcined at 600 and 800°C) and three different carbon loadings were compared.

Carbon loading (%)	Calcination temp. (°C)	Discharge capacity (mAh g^{-1})				Mn^{2+} concentration in electrolyte (m*M*)			Fractional capacity losses from Mn dissolution		
		Initial	20	40	60	20	40	60	20	40	60
21	600	113	82	60	56	0.48	0.61	0.72	0.33	0.23	0.22
	800	127	118	110	105	0.11	0.25	0.43	0.22	0.25	0.30
30	600	117	101	87	74	0.50	0.75	0.88	0.71	0.44	0.35
	800	127	118	112	107	0.23	0.43	0.67	0.50	0.53	0.53
37	600	120	110	101	93	0.53	0.90	1.20	0.83	0.81	0.80
	800	129	122	115	110	0.35	0.58	0.82	0.86	0.79	0.70

already been discussed in the earlier section. With regard to the carbon loading, however, a better cyclability is observed with higher carbon loadings despite extensive manganese dissolution. In addition, the fractional capacity loss contributed by the dissolution steadily increases with carbon content.

The latter two features are now discussed in detail with graphic presentations made with the 600°C spinels (Fig. 7). In Fig. 7a, the dissolved Mn^{2+} contents were plotted against cycle number. As shown, the manganese dissolution was fairly proportional to the carbon content in composite cathodes (also in 800°C fired spinels as referenced in Table III), supporting the premise that solvent molecules are oxidized on carbon surface and an as-generated species plays an active role in the manganese dissolution. However, comparing the results in Fig. 7a and b, the observed capacity losses cannot be directly correlated to the carbon contents, *i.e.*, the material losses. That is, the 37% carbon-loaded cathode shows the best cyclability among the samples even if the material losses are the highest. This implies that material losses alone cannot fully account for the observed capacity losses. As a matter of fact, the results in Fig. 7c indicate that the capacity fade estimated with Mn loss was more than 80% for the 37% carbon-loaded composite electrode, while in the 21% loaded cathode it amounted to only 20 to 40% of the overall loss. Thus, the material loss seems to be the major source for capacity degradation when composite cathodes contain excess carbon (for example, 37% loaded cathode). This is not unreasonable because excess carbon would cause a severe manganese dissolution as described above. However, as the carbon content decreases, the second contribution becomes more important.

The second contribution is likely to come from an increment in cell polarizations which also resulted from the manganese dissolution. Figure 8 shows the 1st and 24th charge/discharge profiles traced with Li/composite cathodes, where spinel oxides fired at 600°C were loaded with the carbon contents of 21 and 37%, respectively. The 1st profiles are similar to each other regardless of the carbon content, and also the well-known two-step charge/discharge profiles[4] can be seen. This shows that the initial cathode properties of the two electrodes are similar to each other. In the 24th profiles, the 37% loaded cathode shows the similar charge/discharge profile with a slight capacity loss. Somewhat differently, however, the 21% carbon-loaded cathode exhibits a big capacity loss due to incomplete charging. During the 24th charging period with this cathode, the charging reaction ended in the middle of the second process since the cell potential had

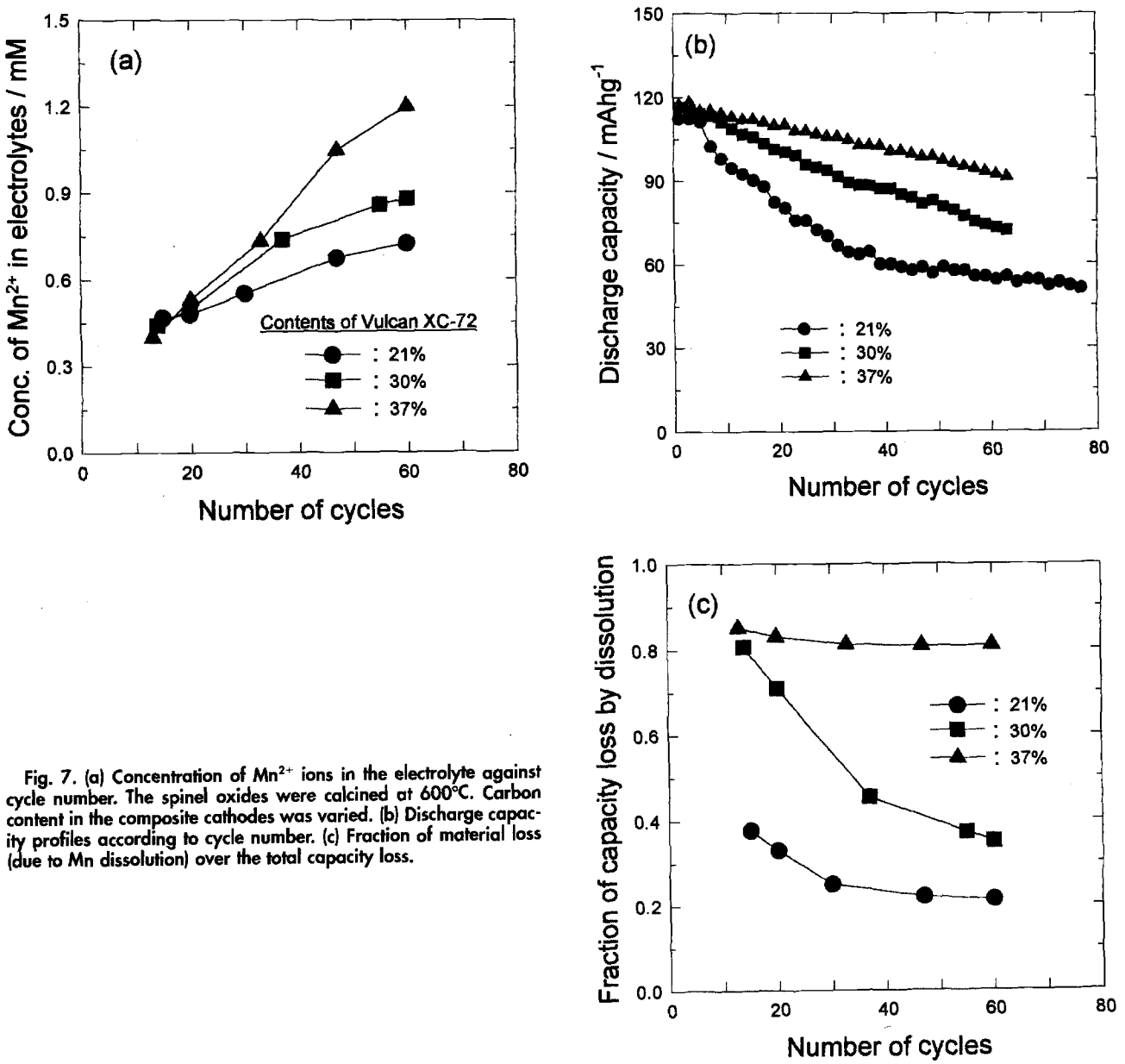

Fig. 7. (a) Concentration of Mn^{2+} ions in the electrolyte against cycle number. The spinel oxides were calcined at 600°C. Carbon content in the composite cathodes was varied. (b) Discharge capacity profiles according to cycle number. (c) Fraction of material loss (due to Mn dissolution) over the total capacity loss.

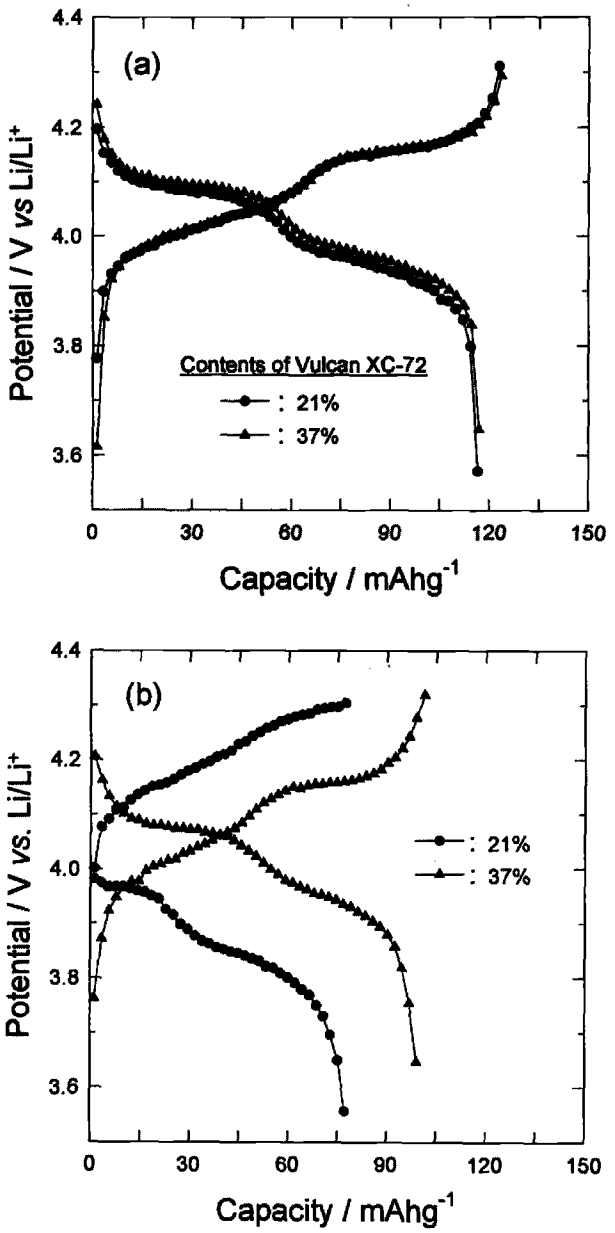

Fig. 8. Charge/discharge profiles of the $Li/Li_xMn_2O_4$ cells. The spinel oxides were prepared by firing at 600°C: (a) the 1st charge/discharge curves and (b) the 24th cycle curves.

reached the cutoff value of 4.3 V. Consequently, the discharge capacity, which should be proportional to the charging capacity, is correspondingly lower. The incomplete charging observed with the 21% carbon cathode can be attributed to a high cell polarization, supposedly, due to an increase in resistances of cell components and/or cell reactions.

Here, a question arises as to why the cell resistances increase with repeated cycling. A clue can be found in the observation that, upon repeated cycling, both the manganese dissolution and capacity losses increase in a parallel way (compare Fig. 1 and Fig. 3a, also Fig. 7a and b). Manganese dissolution would take place at the spinel/electrolyte interface. Then, the surface region of the spinel particles would be Mn-depleted presumably to produce electrochemically inactive spinel layers (defect spinels highly enriched in oxygen), resulting in a high contact resistance at the spinel/carbon interface. The resistances for charge-transfer and/or mass transfer will also be influenced by the manganese dissolution. However, the resistance increments induced by the Mn-depletion depend on the carbon content in the composite electrodes: when composite cathodes contain excess carbon, the initial contact areas (before Mn dissolution) are large enough such that the contact resistance is not greatly altered by Mn dissolution. However, if the carbon contents are low, the contact points would be less abundant such that Mn dissolution would have a greater effect on the contact resistance.

To ascertain this model, the cathodic properties were compared utilizing ac impedance spectroscopy for two composite cathodes loaded with different amounts of carbon. The impedance spectra were obtained with repeated cycling (Fig. 9) and they were fitted with the equivalent circuit depicted in the inset of Fig. 9. The fitted impedance parameters are listed in Table IV. In the equivalent circuit, R_s corresponds to the solution resistance between the reference electrode and the cathode, $R_{contact}$ the contact resistance developed in the composite cathodes, R_{el} the resistance for electrode reactions, Z_W the Warburg impedance, and C_{dl} the double-layer capacitance between current collector and cathode. The R_s values for two cells are slightly different due to a different experimental setup (*i.e.*, distance between the cathode and reference electrode), but even with repeated cycling they remained at their initial values within experimental errors. The Qs are the circuit description code representing the constant-phase element (CPE), which can be expressed in admittance as $Y(\omega) = Y_0 (j\omega)^n$. [22] The nature of the CPE can be determined by the n values. In the present experimental results, n values for Q_1 are close to 1, indicating that Q_1 can be considered as a pure capacitor. The n values for Q_2 are less than 1, which is normally observed in the CPE associated with electrode reactions. The Z_W values slightly decreased along with repeated cycling, but they were too small to be analyzed precisely.

The $R_{contact}$ and R_{el} values are plotted against cycle number in Fig. 10. The initial $R_{contact}$ values (without manganese dissolution) were 0.0 Ω for the 37% carbon loaded cathode and 6.3 Ω for the other. This illustrates that contact points between oxides and carbon particles are well developed in the densely loaded (37%) cathodes, but poorly in the loosely loaded (21%) cathodes. On repeated cycling, the contact resistance increased steadily, but much more rapidly in the 21% loaded cathodes. The similar increasing patterns were observed in R_{el} values. The increment of R_{el} with repeated cycling can be explained by the fact that manganese dissolution also reduces the three-

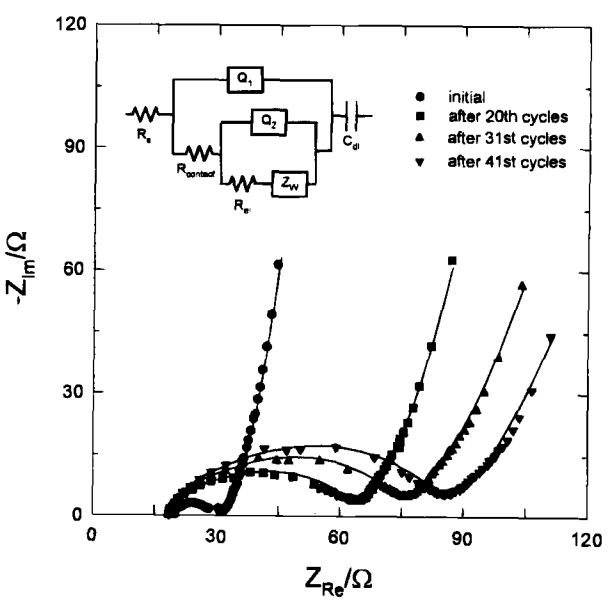

Fig. 9. AC impedance spectra obtained with two composite cathodes of different carbon loadings. The spinel oxide was prepared by firing at 600°C. The solid line indicates the best fit with the equivalent circuit depicted in the inset.

Table IV. Deconvoluted ac impedance parameters as a function of carbon loading and cycle numbers.

Carbon content	Number of cycles	R_s (Ω)	C_{dl} (Farad)	Q_1[a] (Ω^{-1}) Y_0	n	$R_{contact}$ (Ω)	Q_2[a] (Ω^{-1}) Y_0	n	R_{el} (Ω)	Z_W (Ω^{-1})
21%	Initial	20.0	0.10	5.22×10^{-6}	0.95	6.3	1.06×10^{-3}	0.67	4.83	0.11
	20	18.5	0.27	1.01×10^{-5}	0.89	12.7	5.66×10^{-4}	0.58	33.6	0.10
	31	18.5	0.37	1.70×10^{-5}	0.84	17.8	4.05×10^{-4}	0.61	39.9	0.08
	41	18.5	0.55	1.77×10^{-5}	0.84	20.8	3.79×10^{-4}	0.61	47.0	0.09
37%	Initial	15.2	0.17	1.14×10^{-6}	1.0	0.0	1.26×10^{-4}	0.69	6.2	0.18
	18	15.1	0.35	3.50×10^{-6}	1.0	5.0	1.58×10^{-4}	0.68	9.2	0.14
	27	15.6	0.41	3.36×10^{-6}	1.0	5.0	1.35×10^{-4}	0.68	11.7	0.13
	35	15.7	0.46	3.39×10^{-6}	1.0	5.5	8.23×10^{-5}	0.74	12.3	0.11

[a] Q is the circuit description code representing the constant-phase element (CPE). Representation of CPE in admittance is $Y(\omega) = Y_o \cdot (j\omega)^n$.

phase boundary sites (the contact points between oxide, carbon, and electrolyte solution), where the electrode reactions for Li^+ intercalation/deintercalation take place. An increase in $R_{contact}$ and R_{el} will cause a high cell polarization, leading to an incomplete charging and therefore apparent capacity losses.

Conclusion

The purpose of this study was to address the source of cathodic capacity losses encountered in 4 V $Li/Li_xMn_2O_4$ cells. Summarizing the results, several valuable points may be given: (*i*) Jahn-Teller distortion is not an important factor for the capacity losses of spinel manganese oxides in 4 V $Li/Li_xMn_2O_4$ cells. (*ii*) A higher calcination temperature is preferred since the spinel's composition approaches stoichiometric (less contamination by highly oxygen-rich defect spinels). Also, they show better capacity retention in spite of their smaller surface areas because Mn dissolution is less severe. Spinels dissolve into the electrolytes (PC/DME + $LiClO_4$), particularly at the charged state (approaching to 4.3 V). And, in this potential range, solvent molecules are also electrochemically oxidized on a carbon electrode. Combining these results, it has been proposed that Mn dissolution is induced by some intermediates which are generated by an electrochemical oxidation of solvent molecules on the carbon surface. (*iii*) Mn dissolution leads to capacity losses in two different ways; a material loss of the active component (spinel oxides) and a polarization loss resulting from an increment of cell resistances. When the carbon content in composite cathodes is low, Mn dissolution is less severe, but this critically affects the contact areas between oxide and carbon particles, leading to a big increase in contact resistance and electrode reaction resistance. Hence, cell polarization would be the dominant factor for the capacity losses in this cathode. On the other hand, when cathodes contain excessive carbon, the polarization loss is less severe. Instead, material losses due to Mn dissolution account for the major portion of the capacity losses.

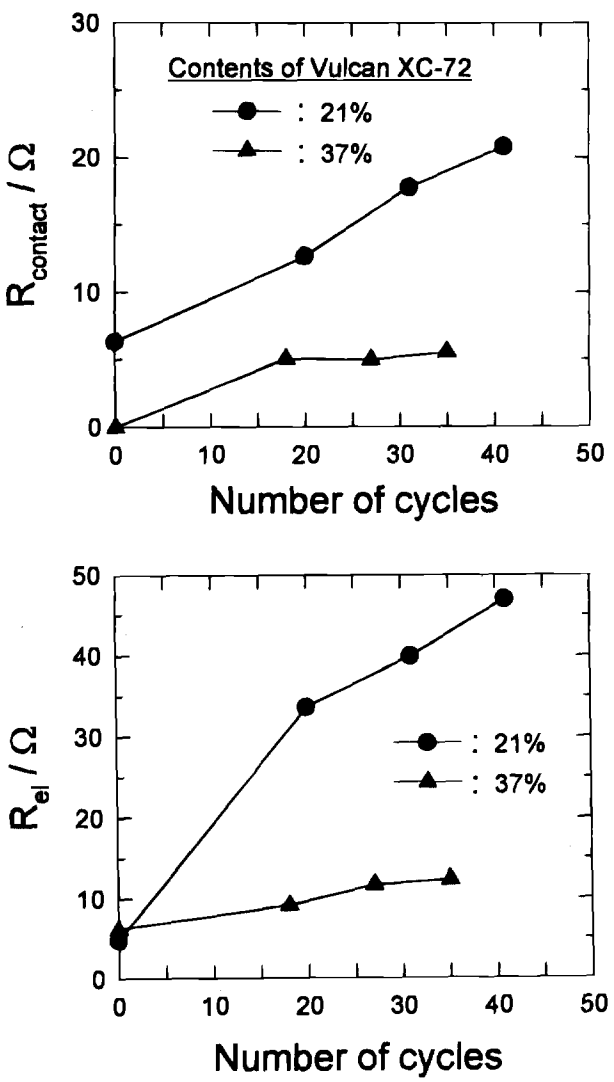

Fig. 10. Evolution of $R_{contact}$ and R_{el} with repeated cycling. Two composite cathodes with different carbon loadings were compared to each other.

Results to date illustrate that cathodic capacity losses in spinel manganese oxides can be determined by several factors: powder properties of spinel oxides (surface areas in particular), solvent composition in the electrolytes, and carbon loadings in the composite cathodes. In this study, investigations have been limited to PC + DME mixture, leaving for future study other solvents or solvent mixtures. Concerning the carbon content, the present results suggest that an addition of excess carbon may be advantageous for cyclability. However, this would in turn be undesirable with respect to the energy and power densities of the resulting batteries. Thus, the carbon loadings in cathodes should be optimized. Finally, carbon additives of different precursors and/or different surface areas should be further examined for their effects on Mn dissolution and polarization losses. These issues will appear in a forthcoming report.

Manuscript submitted Dec. 11, 1995; revised manuscript received March 6, 1996.

REFERENCES

1. G. Pistoia and G. Wang, *Solid State Ionics*, **66**, 135 (1993).
2. L. Chen, X. Huang, E. Kelder, and J. Schoonman, *ibid.*, **76**, 91 (1995).
3. H. Huang and P. G. Bruce, *J. Power Sources*, **54**, 52 (1995).
4. T. Ohzuku, M. Kitagawa, and T. Hirai, *This Journal*, **137**, 769 (1990).
5. J. M. Tarascon, E. Wang, F. K. Shokoohi, W. R. Mckinnon, and S. Colson, *ibid.*, **138**, 2859 (1991).
6. J. M. Tarascon, W. R. Mckinnon, F. Coowar, T. N.

Bowmer, G. Amatucci, and D. Guyomard, *ibid.*, **141,** 1421 (1994).
7. M. M. Thackeray, A. de Kock, M. H. Rossouw, D. Liles, R. Bittihn, and D. Hoge, *ibid.*, **139,** 363 (1992).
8. A. de Kock, M. H. Rossouw, L. A. de Picciotto, M. M. Thackeray, W. I. F. Daivid, and R. M. Ibberson, *Mater. Res. Bull.*, **25,** 657 (1990).
9. M. M. Thackeray, R. J. Gummow, A. de Kock, A. P. de la Harpe, D. C. Liles, and M. H. Rossouw, in *Proceedings of 11th Seminar on Primary and Secondary Battery Technology and Application,* Deerfield Beach, FL, Feb. 1994.
10. G. Pistoia, D. Zane, and Y. Zhang, *This Journal,* **142,** 2551 (1995).
11. J. M. Tarascon and D. Guyomard, *ibid.*, **138,** 2864 (1991).
12. D. Guyomard and J. M. Tarascon, *ibid.*, **139,** 937 (1992).
13. R. J. Gummow, A. de Kock, and M. M. Thackeray, *Solid State Ionics,* **69,** 59 (1994).
14. H.-M. Zhang, Y. Teraoka, and N. Yamazoe, *Chem. Lett.*, 665 (1987).
15. M. S. G. Baythoun and F. R. Sale, *J. Mater. Sci.*, **17,** 2757 (1982).
16. G. H. Jeffery, J. Bassett, J. Mendham, and R. C. Denney, *Vogel's Textbook of Quantitative Chemical Analysis,* 5th ed., p. 584, Longman Scientific & Technical, New York (1989).
17. A. Wattiaux, J. C. Grenier, M. Pouchard, and P. Hagenmuller, *This Journal,* **134,** 1714 (1987).
18. H. Mao, J. N. Reamers, Q. Jhong, and U. von Sacken, in *Proceedings of the Symposium on Rechargeable Lithium and Lithium Ion Batteries,* S. Megahed, B. M. Barnett, and L. Xie, Editors, PV 94-28, pp. 245-250, The Electrochemical Society Proceedings Series, Pennington, NJ (1995).
19. J. M. Tarascon, F. Coowar, G. Amatuci, F. K. Sokoohi, and D. G. Guyomard, *J. Power Sources,* **54,** 103 (1995).
20. D. T. Sawyer and J. L. Roberts, Jr., *Experimental Electrochemistry for Chemists,* pp. 358-382, John Wiley & Sons, Inc., New York (1974).
21. EG&G Princeton Applied Research Application Brief I-1 and Application Note 156.
22. B. A. Boukamp, *Equivalent Circuit Users Manual,* 2nd revised ed., Department of Chemistry, Technical University of Twente.
23. J. Barker, *Electrochim. Acta,* **40,** 1603 (1995).
24. J. Barker and R. Koksbang, *Solid State Ionics,* **78,** 161 (1995).

Molecular Dynamics Studies of Lithium Injection in Model Cathode/Electrolyte Systems

D. T. Kulp and S. H. Garofalini

Department of Ceramics and Interfacial Molecular Science Laboratory, Institute for Engineered Materials, Rutgers, The State University, Piscataway, New Jersey 08855, USA

ABSTRACT

Molecular dynamics simulations of lithium injection in lithium metasilicate-WO_3 systems have been performed. Lithium ion penetration is more prevalent in amorphous WO_3 in comparison to the crystalline form. Migration dynamics can be augmented through an increase in the simulation temperature or by decreasing the coulombic repulsion between the tungsten and lithium ions. For crystalline WO_3, Li^+ injection is dependent on the orientation of the crystal. Lithium penetration is more pronounced for the crystal with the (001) orientation than in the (110) oriented crystal, where there is only limited Li^+ diffusion.

Introduction

Tungsten trioxide thin films (WO_3) have attracted much interest as a cathode material in solid-state electrochemical cells, and more specifically for their electrochromic properties.[1-3] In fact WO_3 was the first electrochromic material discovered.[4] Originally interest was based on applicability to display devices, but with the development of liquid crystal displays, interest has shifted to daylight and solar heat gain management in building windows. Since these applications do not require fast response times, investigators have turned to lithium tungsten bronzes due to their greater room temperature stability. Inorganic electrochromism is based on a change in optical properties, *i.e.*, color changes, due to changes in the charge state of the metal ion. This process is reversible, and can be cycled via a potential pulse. In WO_3, which is colorless, coinsertion of lithium ions with electrons forms a blue nonstoichiometric tungsten bronze. This reversible reaction can be written as follows

$$WO_3 + xLi^+ + xe- \rightleftarrows Li_x WO_3 \qquad [1]$$

where the electron is localized near a tungsten ion, converting the W^{+6} to a W^{+5}.

Though much work has been done investigating the structure and properties of polycrystalline and amorphous WO_3 prior to, after, and during ion insertion,[5-15] few detailed studies have been made into the microscopic nature of the reaction. Several computational studies[16-18] have been carried out on tungstate bronzes, but all have focused on the sodium bronzes. These studies have shown that empirical models can be used to describe adequately the structure of these bronzes and to elucidate some physical properties of these systems. But still the dynamics associated with the transport of ions to and through the electrolyte/WO_3 interface have not been investigated. Understanding the atomic transport mechanisms and the microscopic structure/property relationships within this system will lead to a greater understanding of electrochromic and, more generally, electrolytic interactions in these systems.

In this study, we examine the interfacial dynamics between lithium metasilicate glass, an ionic conductor, and crystalline and amorphous WO_3 using molecular dynamics (MD) computer simulations. The multibody interatomic potential used here was initially developed to simulate bulk silica glass.[19] It is a robust potential which has been successfully applied in simulations of the dynamic and structural properties of alkali silicates,[20] sodium aluminosilicate glasses,[21] glass surfaces,[22] and molecules.[23,24] It has also been used in simulations of the bulk and surfaces of α- and γ-alumina.[25,26] In all cases, results have compared favorably to available experimental data.

In this paper we present simulation results for two investigations of lithium insertion into WO_3. In these systems, a lithium metasilicate glass is used as the solid electrolyte. First we compared the propensity for lithium diffusion from the metasilicate to amorphous (a-WO_3) and